Mechanism for Low Temperature Growth of Boron Nitride Nanotubes

Ming Xie, Jiesheng Wang, and Yoke Khin Yap*

Department of Physics, Michigan Technological University, 1400 Townsend Drive, Houghton, Michigan 49931

Received: May 18, 2010; Revised Manuscript Received: August 24, 2010

Selective growth of boron nitride nanotubes (BNNTs) was demonstrated by plasma-enhanced pulsed laser deposition (PE-PLD). Although PLD is a physical vapor deposition technique for the growth of boron nitride (BN) thin films, ion sputtering induced by the plasma can eliminate the formation of BN thin films and lead to the so-called total resputtering region, in which, a pure phase of BNNTs can be grown at 600−700 °C using Fe catalyst. These BNNTs can be grown at desired locations and have high structural orders with diameter ∼10−20 nm. In addition, we found that effective catalysts for the growth of these BNNTs should have both significant solubility of boron and relatively low sputtering yield. All of these observations can be summarized into a phase selective growth model that combining the vapor−liquid−solid (VLS) mechanism and the effect of ion sputtering.

Introduction

Carbon nanotubes (CNTs) have attracted tremendous research interest due to their unique structural, mechanical, chemical, and electronic properties.[1] However, it is still not possible to grow CNTs with uniform structures and properties. Conversely, boron nitride nanotubes (BNNTs) were predicted to have uniform electronic properties that are not sensitive to their chirality, diameters, and the number of coaxial BN shells.[2] As experimentally confirmed, the band gaps of BNNTs are ranging from ∼5.0 to 6.0 eV.[3] In addition, BNNTs possess piezoelectric properties[4] and high resistance to oxidation.[5] These properties make BNNTs prospective nanomaterials that will complement CNTs for various applications at the cutting edge of nanotechnology.

The difficulty in growing high-purity BNNTs has hindered research progress on BNNTs for more than 10 years. BNNTs can be grown by arc discharge,[6] laser ablation,[7] substitution reactions from carbon nanotubes,[8] ball-milling,[9] and chemical vapor deposition.[10] All of these methods require high growth temperatures (∼1300−3000 °C) or special instrumentation or involve dangerous chemical reactions. The products are mixed with impurities, including amorphous boron nitride powders, catalyst particles, etc. Recently, we demonstrated that pure BNNTs can be grown on Si substrates by using a convention tube furnace without dangerous chemical reaction.[11] This was obtained by applying the so-called growth vapor trapping (GVT) procedure and the chemical route of boron oxide CVD. By applying the same technique, patterned growth of high-purity BNNTs were obtained by using a series of effective catalysts at 1200 °C.[3c] This recent progress has made the growth of BNNTs much like the synthesis of CNTs and nanowires.

In fact, patterned growth of high-purity BNNTs on Si substrates was first achieved in 2005. This was obtained at 600 °C by plasma-enhanced pulsed-laser deposition (PE-PLD).[3a] Recently, microwave plasma CVD were also used for the growth of BNNTs at 800−900 C.[12] The PE-PLD technique is unique for several reasons: (i) It was the first technique for patterned growth of BNNTs with fine tubular structures (not the defective bamboo-structures). (ii) The growth temperatures are significantly lower than those required in all reported techniques. (iii) PE-PLD involves a phase selective growth mechanism, where only pure BNNTs will be grown without BN films (including the hexagonal and cubic phases, *h*-BN and *c*-BN, respectively). Apparently, it is important to further investigate the detailed growth mechanism of PE-PLD. However, there are many growth parameters that require further investigations, such as substrate temperatures, plasma-induced substrate bias-voltages, and catalysts. In this paper, we describe detailed analysis on these growth parameters so as to elucidate the nucleation process and growth mechanism of BNNTs at low temperatures.

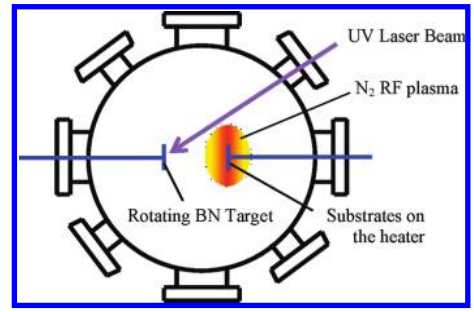

Figure 1. Schematic of the PE-PLD system. Laser beam is focused on a rotating BN target. The BN growth specie from the target will be accelerated toward the substrate by the substrate bias voltages.

Experimental Procedures

The PE-PLD system consists of an ultrahigh vacuum stainless steel chamber (Figure 1) and the fourth harmonic generation (wavelength = 266 nm, pulse duration = 5 ns) of a Nd:YAG laser. Pure iron (13.2 nm) film was first deposited on oxidized silicon substrates (oxide layer ∼120 nm) at room temperature by PLD in vacuum. The thickness of the Fe films was controlled by an in situ monitoring system with an accuracy of 0.1 nm. Substrates with Fe films were then installed on the heater and sealed inside the vacuum chamber at a base pressure as high as $\sim 5 \times 10^{-7}$ mbar (10^{-9} Torr). The chamber was then filled with pure nitrogen (99.998%) gas to a pressure of 5×10^{-2} mbar. The substrates were heated and maintained at 600 °C by a pyrolytic BN heater (Momentive Performance Materials) that

* To whom correspondence should be addressed. E-mail: ykyap@mtu.edu.

10.1021/jp104550j
Published on Web 09/14/2010

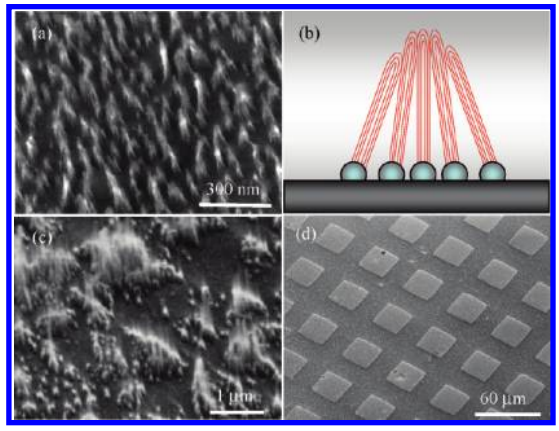

Figure 2. SEM images of BNNT bundles (a, c, and d) and the schematic of a bundle (b).

was controlled by a proportional-integration-differentiation (PID) system. Plasma was generated on the substrate surface for 10 min by an RF generator (13.56 MHz) that was capacitively coupled on the steel substrate holder. This RF plasma induced negative dc voltages on the substrates (substrate bias).[13] Then deposition of BNNTs was initiated by focusing the laser beam onto a high purity h-BN target (grade HBC, GE Advanced Ceramics). The laser intensity during ablation was ~0.2 GW/cm^2 on the target surface. The BN vapor then propagated toward the substrates located ~4 cm from the target surface.

Results and Discussion

I. Patterned Growth of BNNTs. Figure 2 shows the typical scanning electron microscopy (SEM) images of BNNTs grown by PE-PLD. As shown in Figure 2a, these BNNTs tend to form vertical conical bundles. Each bundle consists of multiple BNNTs grown according to the base-growth mode as schematically illustrated in Figure 2b. The blur appearance of the BNNTs is due to (1) the charging effect of the insulating BNNTs under the electron beam irradiation, (2) bundling of small diameter (~10−20 nm) BNNTs, and (3) the fact that no catalyst particles are remained along the BNNTs. We think that the tendency of forming vertical conical bundles is due to two main reasons: (1) the plasma induced electric field in the direction perpendicular to the substrate surface and (2) the relatively larger distances between effective catalyst particles due to plasma etching. As shown in Figure 2c, the length of these BNNTs can be as long as 1 μm at substrate locations in contact with the holder due to higher plasma density. In addition, the growth location of these BNNT bundles can be precisely controlled as shown in Figure 2d. These regular arrays of BNNTs can be formed by using patterned Fe films created by shadow masks. This result illustrates that the growth locations of BNNTs are controlled by the locations of the Fe nanoparticles, the typical catalytic growth manner of CNTs by CVD techniques.[14]

Transmission electron microscopy (TEM) was used to examine the structure of the BNNTs. Long and straight tubular structures were detected as shown in Figure 3a,b. The tips of these BNNTs were fully capped with no evidence of catalyst particles. This observation indicates that base-growth mechanism is responsible for the growth of BNNT bundles, consistent with our interpretation on their SEM images discussed earlier. Electron diffraction of the (002) and (004) planes of BNNTs are shown in the inset. The magnified image (Figure 3b) indicates that these BNNTs have an intershell spacing of ~0.34 nm. It is worth noting that the internal tubular channels of these BNNTs are very small (~1 nm), much smaller than those ever detected from BNNTs grown by CVD. Raman spectroscopy was also used to characterize these BNNTs. These were done by a con-focal Raman microscope with a UV excitation laser (HeCd, λ = 325 nm). A sharp Raman peak at ~1369 cm^{-1} was detected (inset of Figure 3a), which is corresponding to the E_{2g} in-plane vibrational mode of the h-BN networks. This Raman signal is well recognized as the fingerprint of BNNTs as regularly confirmed by our diffraction patterns, electron energy loss spectroscopy (EELS), and infrared spectroscopy.[3c,11]

Although we have previously proposed a preliminary growth model for the formation of these BNNTs,[3a] the detailed effects of some essential growth parameters were not clearly established. Thus a series of experiments are conducted systematically to assist better understanding on the nucleation and the subsequent growth mechanism of these BNNTs.

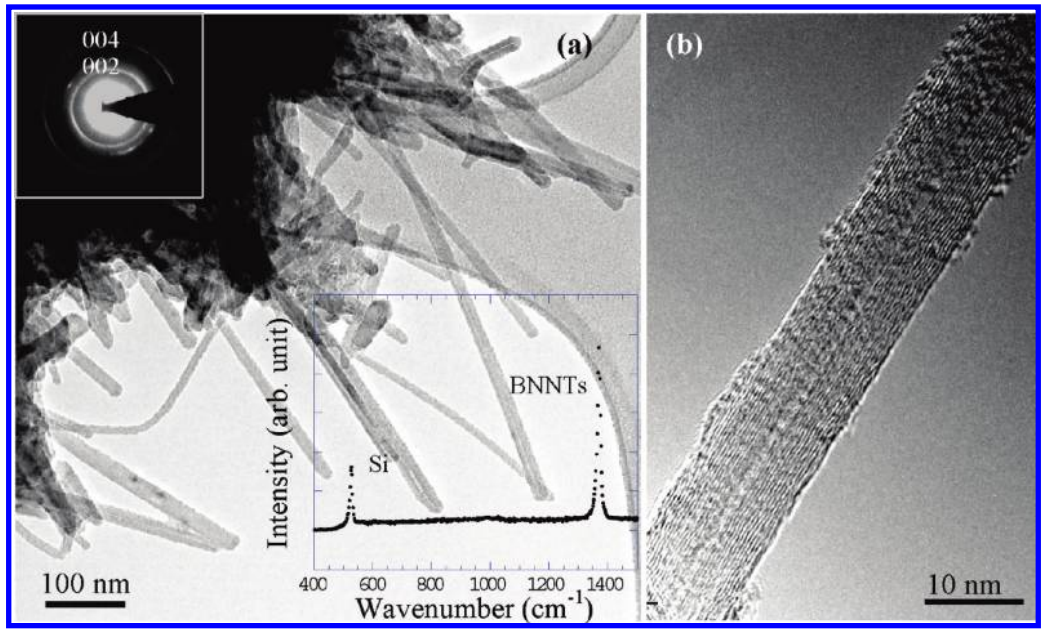

Figure 3. TEM images of BNNTs at (a) low and (b) high magnification. Electron diffraction pattern and Raman spectra of BNNTs are shown in the insets.

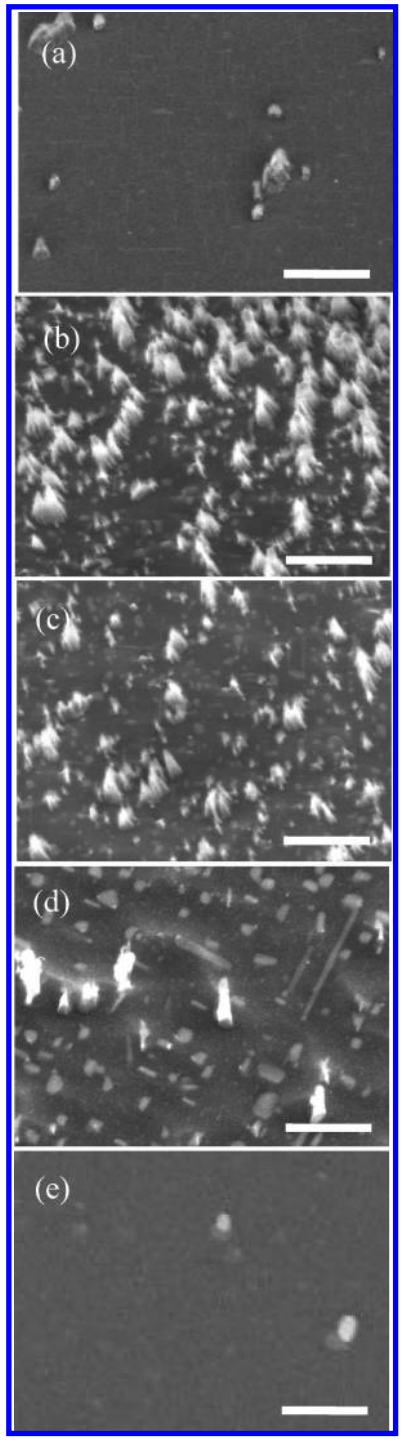

Figure 4. Growth morphologies of samples grown at substrate temperatures of (a) 500, (b) 600, (c) 700, (d) 800, and (e) 900 °C. All scale bars are 600 nm.

II. Effects of the Substrate Temperatures. The patterned growth of these BNNTs indicates that the vapor−liquid−solid (VLS) process on Fe catalysts is responsible for the growth mechanism. Since the solubility of BN growth species in Fe catalysts is depend on the growth temperatures, we have thus investigated their effects on the growth of BNNTs. This series of experiments were conducted at a substrate bias voltage of −380 V and other growth parameters were kept the same as described in the experimental procedures. As shown in Figure 4b,c, BNNTs can be grown on Si substrates at a narrow temperature range from ∼600 to 700 °C. Very few BNNTs were formed at the temperatures beyond this range [Figure 4a,d,e]. Apparently, a minimum temperature is required for the growth of BNNTs and can be explained either by the minimum temperature requirement for sufficient diffusion and solubility of BN species in Fe catalyst or the activation energy to overcome the strain energy needed to form nanotubular structures with large curvature of the BN shells. On the other hand, when the temperature rises above 700 °C (Figure 4d,e), several possibilities may hinder the growth of BNNTs: (1) excessive reaction between iron and the oxidized silicon substrate to produce iron silicides which may not be catalytic for BNNT growth and (2) the evaporation of iron nanoparticles with the assistance of plasma heating. Experimentally, we found that BNNTs can not be grown when Si substrates were used without the silicon oxide diffusion barriers, probably due to the formation of iron silicides. It is noted that all of the substrate temperatures were measured by a thermocouple in contact with the surface of the substrates. The actual temperatures on the Fe catalysts may be higher due to plasma heating effects.

III. Effects of the Substrate Bias Voltages. In fact, the growth of BNNTs by PE-PLD strongly depends on the substrate negative bias voltages. The effect of substrate biasing was examined by growing a series of BNNT samples at 600 °C with other growth parameters unchanged as described in the experimental procedures. One of the intentions to apply a negative bias voltage is to increase the kinetic energy of the positive ionic species in the laser plume and the nitrogen plasma (B^+, B^{2+}, N^+, N_2^+, N_3^+, etc.). We aimed at preventing the formation of BN thin films by the ion bombardments and resputtering process. We think that BN films will prevent the formation of BNNTs. This is analogous to the catalyst poisoning effect in the formation of amorphous carbon films during the growth of CNTs.[15]

When the bias voltages are between 0 to −300 V, the deposition rate of BN films is faster than the resputtering rate of the deposited films by ion bombardments. The BN deposition rate is also higher than the diffusion rate of the BN growth species into Fe catalysts. Thus BN films coated on the catalyst terminate the contact between Fe and the reactive growth species as shown in Figure 5a. The range of bias voltages for thin film formation is also consistent with the deposition of hexagonal (h-BN) and cubic phase (c-BN) thin films reported previously.[16]

At negative bias voltages of −350 V and −400 V, the formation of BNNTs is detected as shown in Figure 5, panels b and c, respectively. Apparently the formation of BN thin films was suppressed as the resputtering rate of the deposited film by ion bombardment is sufficient to reach the so-called total resputtering condition, where all deposited BN species are resputtered away from the substrates. This means, the resputtering and the deposition processes have reached to the equilibrium. The reactive BN growth species are always in contact with Fe catalysts to promote the diffusion and dissolution of BN species into Fe nanoparticles. According to the VLS mechanism, this will lead to supersaturation of the BN species and the subsequent segregation from Fe nanoparticles as BNNTs. As the substrate temperatures are still too low to melt the Fe nanoparticles, we think that local plasma heating contributes to the formation of liquid phase near the surfaces of Fe nanoparticles. This is analogous to the solid-core model proposed for low temperature growth of CNTs where exothermic dissociative adsorption produces local heating to form near-surface liquid phase needed for the VLS processes.[15] For BNNTs, a possible plasma-heating mechanism is the subimplantation of BN species into the Fe catalysts. Since the kinetic energy of these BN species is high, this energy can be dissipated

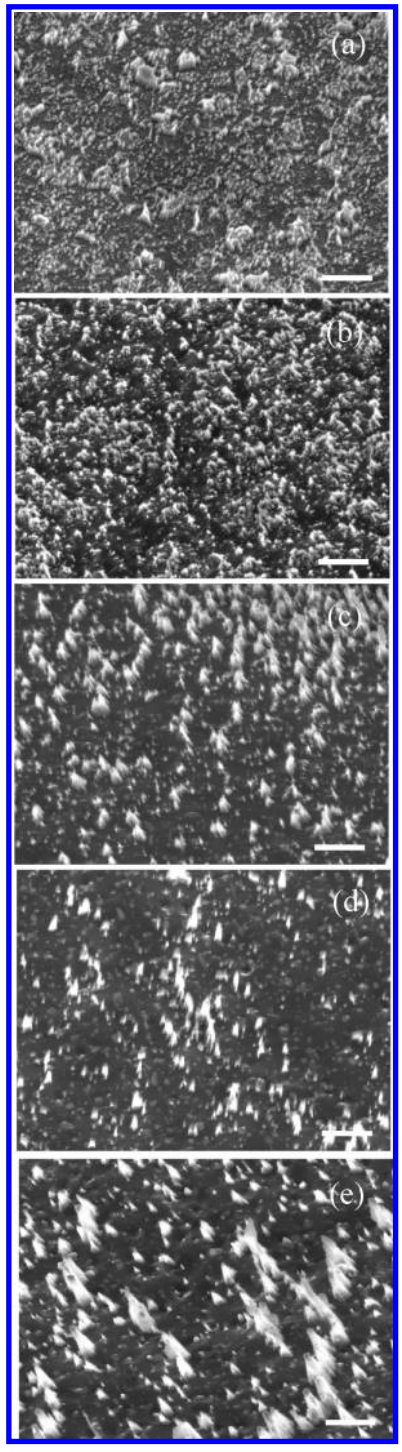

Figure 5. Growth morphologies at substrate bias voltages of (a) −300, (b) −350, (c) −400, (d) −450, and (e) −550 V. All scale bars are 600 nm.

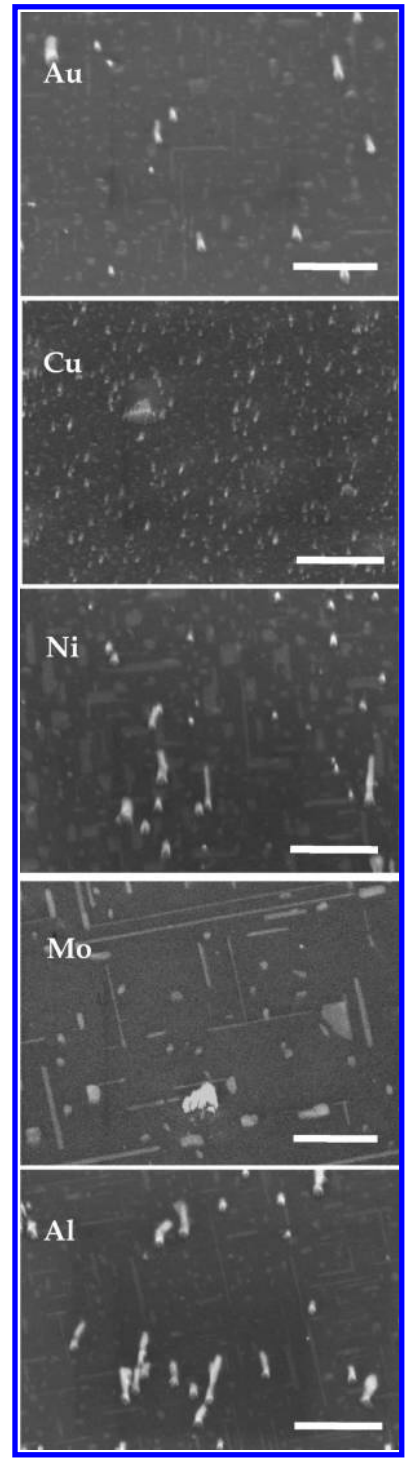

Figure 6. Growth morphologies by using various catalysts. All scale bars are 600 nm.

to the Fe catalysts and substrates and cause local heating. At higher negative biasing of −450 V, the density of BNNTs is reduced [Figure 5d]. We think that this is due to the reduced density of Fe nanoparticles on the substrates due to excessive ion sputtering. At even higher negative biasing of −550 V [Figure 5e], some thick rod-like features can sometime be detected. We think that these are not BNNTs and may be some kinds of Si nanostructures including Si nanotubes that we previously reported.[17]

IV. Effects of the Catalysts. The growth mechanism discussed so far has included the ion sputtering and VLS processes. It is thus desired to provide further evidence to support these discussions. We have thus examined various metallic catalysts to test their catalytic activities for the growth of BNNTs by PE-PLD. These metals are chosen for their differences in (1) sputtering yields and (2) solubility of boron. In this way, both the ion sputtering and VLS factors can be elucidated.

The growth of CNTs has been commonly accepted to follow the VLS growth mechanism, which involves the use of appropriate catalysts. Pt, Pd, Co, Fe, and Ni are well-known for their catalytic function of forming graphitic structures.[19] Au and Cu, however, are less explored but were recently used to grow single walled CNTs.[20] Since graphite and h-BN are iso-

TABLE 1: Physical Properties and Boron Concentration of Bulk Metals[18]

	Au	Cu	Ni	Mo	Fe	Al
sputtering yields	7.4 ± 0.1	3.0 ± 0.4	1.0 ± 0.1	0.82 ± 0.09	0.57 ± 0.01	0.52 ± 0.13
melting points	1064.18 °C	1084.62 °C	1455 °C	2623 °C	1538 °C	660.32 °C
boron concentration in bulk metal (at. %) at T_{alloy} ~600 °C	unknown	unknown	25	unknown	32.5	unknown

electronic, we have thus examined some of these metals for our PE-PLD experiments.

A series of samples were deposited by using the optimum parameters for the growth of BNNTs discussed so far with Fe catalysts. Thus 13.2 nm of Au, Cu, Ni, Mo, and Al were deposited onto the oxidized Si substrates as the catalysts, respectively. The growth morphologies of these samples were examined by SEM and shown in Figure 6. As shown, there is no obvious growth of BNNTs in these cases. This result can be explained by referring to the sputtering yields, melting points of these metals, and solubility of boron in these metals (Table 1). The sputtering yields of metals have been measured by various ions.[21] For instance, Tsunoyama et al., measured the sputtering yields of metals under 20 keV O_2 bombardment. In general, Au has the largest sputtering yield, following by Cu, Ni, Mo, Fe, and Al. This means Au and Cu are easier to be sputtered off by the nitrogen ions and are thus not the ideal catalysts for the growth of BNNTs by PE-PLD. Ni and Mo have similar sputtering yields but about twice higher than that of Fe and Al. However, the melting point of Mo is too high (2623 °C) for the growth of BNNTs at low temperatures described here. Thus, the potential catalysts are Ni, Fe, and Al.

Let us evaluate Ni, Fe, and Al in terms of B and N solubility. The solubility of boron in bulk Ni is comparable to that in Fe. However, Ni tends to be sputtered about twice faster than Fe, causing no effective growth of BNNTs under the growth conditions tested here. Al has sputtering yield similar to Fe and has much lower melting point (660.37 °C). However, we did not obtain effective growth of BNNTs using Al catalysts. We think that this could be due to the low boron solubility in Al, which is not well reported. The solubility of boron in bulk Au, Cu, and Mo are also not well documented. Finally, some unknown nanostructures were detected in cases shown in Figure 6 and will be subjected for further study in the future.

V. Phase Selective Growth Model. To summarize our discussion, we propose a phase diagram (Figure 7) and a schematic growth model (Figure 8) for the formation of BNNTs by PE-PLD. It is well accepted that the formation of *h*-BN and *c*-BN thin films depends on the ratio of ionic to nonionic growth species, *F*, and the kinetic energy of the ionic species, *K*.[16,22] These relations can be summarized in Figure 7. As shown, at particular *F* value, the phases of BN films will be determined by the kinetic energy *K*. At low kinetic energy, only *h*-BN films will be deposited. At higher kinetic energy, *h*-BN films will be suppressed and *c*-BN films will be formed. At even higher kinetic energy, one will reach the total resputtering region where almost no BN thin films will be deposited. Our discovery is that the BNNT phase is located around the total-resputtering region when Fe catalysts are introduced.

Apparently, PE-PLD is a unique technique where the deposition rate, the ratio of ionic to nonionic growth species, *F*, and the kinetic energy of the ionic species, *K*, are controllable in certain extent. The laser ablation process of the BN target is a complex process known as Coulomb explosion.[23] In brief, the strong electrical field generated by the laser light will first remove the electrons from the BN bonds. These free electrons oscillate within the electromagnetic field of the laser light and will collide with the B and N atoms in the target and transfer their energy to the BN lattice. The surface of BN target is then heated up and the material will be vaporized. The temperature of the generated plasma plume is typically 10 000 K.[23] Thus the BN growth species from the target will have high kinetic energy. The deposition rate and the *F* value of BN species can be controlled by the laser pulsed energy. The negative substrate biasing induced by the RF-plasma could further accelerate these ionic species (B^+, B^{2+}, N^+, N_2^+, N_3^+, etc.) and enhance their *F* value and kinetic energies. These growth species has the capability to (1) cause ion sputtering and (2) penetrate onto the growth surface, commonly known as subimplantation mechanism.[22] As shown in Figure 8a,b, ion sputtering will cause the formation of smaller Fe catalyst. Concurrently, subimplantation and ion sputtering will cause local plasma heating and lead to the formation of liquid phase near the surface of the Fe nanoparticles. The subimplantation process also enhances the diffusion of BN species into the near surface liquid region (Figure 8c). Eventually, this will lead to the supersaturation of BN species in the Fe catalyst (Figure 8d). According to the VLS mechanism, segregation (nucleation) of BN species as BNNTs

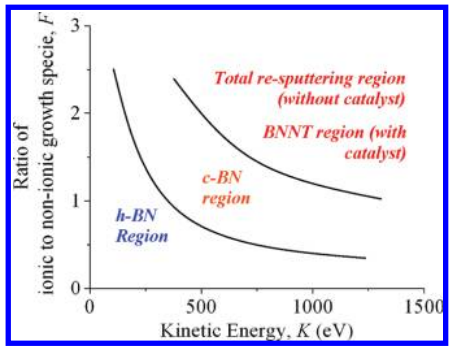

Figure 7. Phase diagram of h-BN, c-BN, and BNNTs.

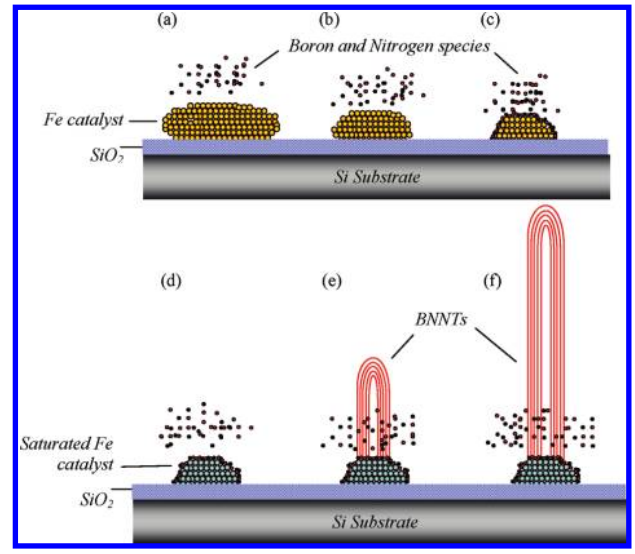

Figure 8. Schematic of the phase selective growth model for BNNTs.

will then occurred (Figure 8e) and lead to the growth of BNNTs (Figure 8f). We believed that the directional and energetic growth species in our PE-PLD technique are important for the formation of highly crystallized BNNTs reported here, without which, will lead to the growth of defective BNNTs as demonstrated in microwave plasma CVD approach.[12]

This growth model also explained the reasons where Au and Cu are not suitable for the growth of BNNTs by PE-PLD. This is due to the fast sputtering rate of these metals, which could not survived to the stage of supersaturation, segregation, and nucleation of BNNTs. The formation of BNNTs by PE-PLD also affected by the solubility of BN growth species into the catalyst and the melting points of the catalyst. For example, Ni has a comparable solubility of BN species as for Fe, however, thicker Ni films will be needed to compensate the higher sputtering yield of Ni. Thicker films and higher growth temperatures will also be needed for Mo to induce the growth of BNNTs even if Mo will have comparable boron solubility as in Fe.

Conclusion

The nucleation and growth of BNNTs by PE-PLD has been systematically studied. Specifically, we have investigated the effect of growth temperatures, bias voltages, and catalysts for the growth of BNNTs. All of the experimental observations can be explained by a phase-selective growth model that includes both the ion sputtering and VLS processes.

Acknowledgment. This project is supported by National Science Foundation CAREER award (Award No. 0447555), the U.S. Department of Energy, the Office of Basic Energy Sciences (Grant DE-FG02-06ER46294), and the Center for Nanophase Materials Sciences sponsored by the Division of Materials Sciences and Engineering, U.S. Department of Energy, under Contract No. DE-AC05-00OR22725 with UT-Battelle, LLC. We also acknowledged contributions from Zhengwei Pan and David Geohegan.

References and Notes

(1) Iijima, S. *Nature* **1991**, *354* (6348), 56.

(2) (a) Rubio, A.; Corkill, J. L.; Cohen, M. L. *Phys. Rev. B* **1994**, *49* (7), 5081. (b) Blase, X.; Rubio, A.; Louie, S. G.; Cohen, M. L. *Europhys. Lett.* **1994**, *28* (5), 335.

(3) (a) Wang, J. S.; Kayastha, V. K.; Yap, Y. K.; Fan, Z. Y.; Lu, J. G.; Pan, Z. W.; Ivanov, I. N.; Puretzky, A. A.; Geohegan, D. B. *Nano Lett.* **2005**, *5* (12), 2528. (b) Arenal, R.; Stephan, O.; Kociak, M.; Taverna, D.; Loiseau, A.; Colliex, C. *Phys. Rev. Lett.* **2005**, *95* (12), 127601. (c) Lee, C. H.; Xie, M.; Kayastha, V.; Wang, J.; Yap, Y. K. *Chem. Mater.* **2010**, *22*, 1782.

(4) (a) Mele, E. J.; Kral, P. *Phys. Rev. Lett.* **2002**, *88* (5), 056803. (b) Nakhmanson, S. M.; Calzolari, A.; Meunier, V.; Bernholc, J.; Nardelli, M. B. *Phys. Rev. B* **2003**, *67* (23), 235406.

(5) Golberg, D.; Bando, Y.; Kurashima, K.; Sato, T. *Scr. Mater.* **2001**, *44* (8−9), 1561.

(6) (a) Terrones, M.; Hsu, W. K.; Terrones, H.; Zhang, J. P.; Ramos, S.; Hare, J. P.; Castillo, R.; Prassides, K.; Cheetham, A. K.; Kroto, H. W.; Walton, D. R. M. *Chem. Phys. Lett.* **1996**, *259* (5−6), 568. (b) Loiseau, A.; Willaime, F.; Demoncy, N.; Hug, G.; Pascard, H. *Phys. Rev. Lett.* **1996**, *76* (25), 4737. (c) Chopra, N. G.; Luyken, R. J.; Cherrey, K.; Crespi, V. H.; Cohen, M. L.; Louie, S. G.; Zettl, A. *Science* **1995**, *269* (5226), 966.

(7) (a) Yu, D. P.; Sun, X. S.; Lee, C. S.; Bello, I.; Lee, S. T.; Gu, H. D.; Leung, K. M.; Zhou, G. W.; Dong, Z. F.; Zhang, Z. *Appl. Phys. Lett.* **1998**, *72* (16), 1966. (b) Lee, R. S.; Gavillet, J.; Chapelle, M. L. d. l.; Loiseau, A.; Cochon, J. L.; Pigache, D.; Thibault, J.; Willaime, F. *Phys. Rev. B* **2001**, *64* (12), 121405.

(8) Han, W. Q.; Bando, Y.; Kurashima, K.; Sato, T. *Appl. Phys. Lett.* **1998**, *73* (21), 3085.

(9) Chen, Y.; Conway, M.; Williams, J. S.; Zou, J. *J. Mater. Res.* **2002**, *17* (8), 1896.

(10) (a) Lourie, O. R.; Jones, C. R.; Bartlett, B. M.; Gibbons, P. C.; Ruoff, R. S.; Buhro, W. E. *Chem. Mater.* **2000**, *12* (7), 1808. (b) Tang, C.; Bando, Y.; Sato, T.; Kurashima, K. *Chem. Commun.* **2002**, (12), 1290.

(11) Lee, C. H.; Wang, J.; Kayatsha, V. K.; Huang, J. Y.; Yap, Y. K. *Nanotechnology* **2008**, *19* (45), 455605.

(12) (a) Su, C. Y.; Juang, Z. Y.; Chen, K. F.; Cheng, B. M.; Chen, F. R.; Leou, K. C.; Tsai, C. H. *J. Phys. Chem. C* **2009**, *113* (33), 14681. (b) Guo, L.; Singh, R. N. *Nanotechnology* **2008**, *19* (6), 065601.

(13) Yap, Y. K.; Kida, S.; Aoyama, T.; Mori, Y.; Sasaki, T. *Appl. Phys. Lett.* **1998**, *73* (7), 915.

(14) (a) Kayastha, V. K.; Yap, Y. K.; Pan, Z.; Ivanov, I. N.; Puretzky, A. A.; Geohegan, D. B. *Appl. Phys. Lett.* **2005**, *86* (25), 253105. (b) Kayastha, V. K.; Wu, S.; Moscatello, J.; Yap, Y. K. *J. Phys. Chem. C* **2007**, *111* (28), 10158.

(15) Kayastha, V.; Yap, Y. K.; Dimovski, S.; Gogotsi, Y. *Appl. Phys. Lett.* **2004**, *85* (15), 3265.

(16) Wang, J. S.; Yap, Y. K. *Diamond Relat. Mater.* **2006**, *15* (2−3), 444.

(17) Xie, M.; Wang, J. S.; Fan, Z. Y.; Lu, J. G.; Yap, Y. K. *Nanotechnology* **2008**, *19* (36), 365609.

(18) Massalski, T. B.; Okamoto, H.; *ASM International., Binary alloy phase diagrams*, 2nd ed.; ASM International: Materials Park, OH, 1990.

(19) Hamilton, J. C.; Blakely, J. M. *Surf. Sci.* **1980**, *91* (1), 199.

(20) Takagi, D.; Homma, Y.; Hibino, H.; Suzuki, S.; Kobayashi, Y. *Nano Lett.* **2006**, *6* (12), 2642.

(21) (a) Tsunoyama, K.; Suzuki, T.; Ohashi, Y.; Kishidaka, H. *Surf. Interface Anal.* **1980**, *2* (6), 212. (b) Yoshitake, M.; Yamauchi, Y.; Bose, C. *Surf. Interface Anal.* **2004**, *36* (8), 801.

(22) Mirkarimi, P. B.; McCarty, K. F.; Medlin, D. L. *Mater. Sci. Eng. R* **1997**, *21* (2), 47.

(23) Chrisey, D. B.; Hubler, G. K. *Pulsed laser deposition of thin films*; J. Wiley: New York, 1994.

JP104550J